Droplets of structured fluid on a flat substrate

Jaeup U. Kim†* and Mark W. Matsen

Received 13th March 2009, Accepted 29th April 2009
First published as an Advance Article on the web 22nd June 2009
DOI: 10.1039/b905163e

We study the equilibrium morphology of droplets of symmetric AB diblock copolymer on a flat substrate. Using self-consistent field theory (SCFT), we provide the first predictions for the equilibrium droplet shape and its internal structure. When the substrate affinity for the A component, η_A, is small, the droplet adopts a nearly spherical shape much like that of simple fluids. Inside the spherical droplet, however, concentric circular lamellar layers stack on top of each other; hence the thickness of the droplet is effectively quantized by a half-integer or integer number of layers. At larger η_A and smaller contact angle, the area of the upper-most layer becomes relatively large, resulting in a nearly flat, faceted top surface, followed by a semi-spherical slope. This geometry is remarkably reminiscent of the droplet shapes observed with smectic liquid crystals.

I. Introduction

For the past few decades, the morphological behavior of diblock copolymer mixtures has been the subject of intense experimental and theoretical studies,[1] and various simple and complex phases have been theoretically identified.[1–4] Most of these efforts have focused on the bulk block copolymer phase behavior. The block copolymer phase diagram is now well established, and with the emergence of nanoscience, researchers are turning their attention to block copolymers in confined geometries which exhibit much richer phase behaviors.[4] For example, corrugated surfaces help create almost perfectly aligned block copolymer domains,[5–7] and cylindrical and spherical confinement is known to produce a vast number of new block copolymer phases that are not present in the bulk phase diagram.[8,9] Because these systems use rigid confinement, a natural approach is to assume incompressible polymer melt statistics with reflective walls located at the polymer surface and, if necessary, an associated surface interaction energy is considered.

If no such confinement is imposed, the polymer material will adjust its shape in response to the internal morphology. This is arguably a more fundamental problem than the confinement studies, but it has nevertheless escaped serious attention until just recently; Croll *et al.*[10] observed that a symmetric diblock copolymer droplet self-assembles into a stack of concentric circular disks with a terraced profile (see Fig. 1b) within a hyperbolic envelope. This contrasts the behavior of simple liquids which form a spherical cap on the substrate with a contact angle, θ, determined by the relative surface tensions (see Fig. 1a). The AFM measurements of the block copolymer droplets strongly suggest that circular lamellar layers stack on top of each other as schematically drawn in Fig. 1b. Croll *et al.* also developed a simple phenomenological model in which the surface tension and inter-layer potential compete to determine the droplet shape. Even though it successfully predicted a hyperbolic droplet shape, this result relies on a number of assumptions. Here we aim to do away with any such assumptions by using a coarse-grained microscopic theory.

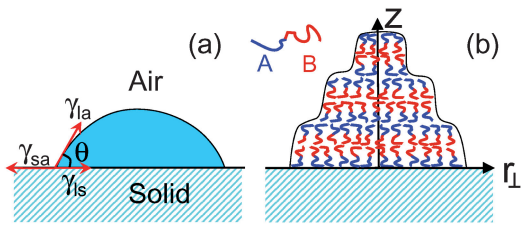

Fig. 1 (a) A liquid droplet on a solid substrate surrounded by air. The liquid–air (γ_{la}), solid–air (γ_{sa}), and liquid–solid (γ_{ls}) surface tensions determine the contact angle by Young's equation, $\gamma_{la}\cos\theta + \gamma_{ls} = \gamma_{sa}$, which is the lateral force balance equation. (b) Schematic diagram of a symmetric ($f = 0.5$) AB diblock copolymer droplet with 3 periods of circular lamellar layers in a terraced geometry (side view).

Interestingly, another complex fluid with internal structure, smectic A liquid crystal, is known to adopt a different geometry on a flat substrate.[11,12] Smectic A liquid crystal has a tendency to form lamellar layers analogous to those of the symmetric block copolymers but with a thickness that is an order of magnitude smaller. The liquid crystalline layers tend to align parallel to the substrate and free surface, but it is impossible to satisfy this condition at both droplet boundaries without creating internal defects. It has been reported that such a droplet adopts a flat top surface connected to a curved side surface making contact with the substrate; hence it is referred to as a *faceted* droplet. A stack of circular liquid crystal disks analogous to Fig. 1b is one candidate for its internal structure, but it inevitably imposes a high energy penalty at the side surface.[11] One can imagine another structure where the layers are parallel to both the air and substrate surface.[12] This morphology reduces the surface energy, but it requires the creation of internal defects which are energetically costly; thus, it is not obvious which morphology is favorable. Unfortunately, the detailed structure could not be identified because the typical liquid crystal layer thickness was too small to resolve. Thus, the study of the block copolymer droplets, whose domain size is more than one order of magnitude larger, may provide a clue to understanding the liquid crystal droplets.

Department of Mathematics, University of Reading, Whiteknights, Reading, RG6 6AX, UK
† Present address: School of Mechanical and Advanced Materials Engineering, UNIST, Korea. E-mail: jukim@unist.ac.uk

In this report, we solve the polymer droplet morphology using SCFT, a theory constructed from first principles. It is well known for providing quantitatively reliable predictions. However, the traditional SCFT framework does not deal with surfaces where the segment density drops to zero on the nanometer length scale. A few attempts have been made to incorporate the density transitional feature into SCFT. One simple approach is to fill the surrounding volume with solvent competing for the space with polymers,[13–15] and generalization to a 2-dimensional system has also been formulated.[16] However, this method inevitably introduces the solvent entropy which does not have a physical ground. Another well known method is to remove the incompressibility condition and add a polymer density dependent potential term to the self-consistent field. A simple quadratic potential[17,18] and a more sophisticated potential from density functional theory[17,19] have been tried. In this approach, the potential originates from other analytical or phenomenological theory, and the result depends on its choice.

Here, we choose a simplified but nevertheless reasonable approach with minimal external parameters. As long as the surface layer is much thinner than both the block copolymer domain size and curvature, the explicit contribution from the surface region reduces to a surface energy which is proportional to area. This property can be easily implemented by filling the air region with a uniform background of long homopolymer chains. Their penetration into the droplet is well known to attenuate with a hyperbolic tangent function. Unlike the case of added solvent, the entropic effect diminishes for infinitely long homopolymers. As a result, the only free parameter we introduce is the χ parameter which is directly related to the surface tension, $\gamma = k_B T a \rho_0 \sqrt{\chi/6}$, where ρ_0^{-1} is the volume of a segment.

The outline of the paper is as follows. In section II, we introduce our theoretical model of the droplet and its implementation using the real-space SCFT method. In section III, we first present droplet shapes as a function of the polymer–substrate attraction. The droplet spreads as the attraction increases, but the detailed morphology strongly depends on if the air prefers to have contact with one of the domains or not. Later, we show various metastable structures which might be observable in experiments, and we explain the complicated nature of the droplet spreading. In section IV, the theoretical result is compared with the known experimental system of Croll *et al.*, and the origin of the difference is discussed. Section V concludes with a brief summary.

II. Theory and droplet modeling

Our model system includes two types of chains, AB block copolymers and long homopolymers (h). Using the standard SCFT method,[20,21] the block copolymers are treated as Gaussian chains with a natural end-to-end length $aN^{1/2}$ where a is the statistical segment length and N is the number of segments per chain. The mean field acting on each segment type is self-consistently determined by the segment densities, ϕ_A, ϕ_B, and ϕ_h:

$$w_i(\mathbf{r}) = -2\eta_i \delta(z) a N^{1/2} + \xi(\mathbf{r}) + \sum_{j \neq i} \chi_{ij} N \phi_j(\mathbf{r}) \qquad (1)$$

where the Flory–Huggins parameters χ_{ij} specify the interaction strength between i and j type segments (i and j are A, B or h). The delta function imposes an interaction energy between the segments and substrate at $z = 0$ ($-\Lambda N$ is often used instead of η; see ref. 22) and $\xi(\mathbf{r})$ is the pressure field that enforces incompressibility,

$$\phi_{tot}(\mathbf{r}) = \sum_i \phi_i(\mathbf{r}) = 1 \qquad (2)$$

The block copolymer statistics are calculated by solving the partition function for a chain fragment of sN segments, $q(\mathbf{r},s)$, where s follows the polymer backbone from 0 at the A end to 1 at the B end. It is efficiently evaluated by solving a modified diffusion equation,[23,24]

$$\frac{\partial}{\partial s} q(\mathbf{r}, s) = \left[\frac{a^2 N}{6} \nabla^2 - w(\mathbf{r}) \right] q(\mathbf{r}, s) \qquad (3)$$

subject to the free chain-end initial condition, $q(\mathbf{r},0) = 1$.[20] The field switches from w_A to w_B at the AB junction point, $s = f$.

Then, a conjugate partition function, $q^\dagger(\mathbf{r},s)$, representing the other fragment of the block copolymer is evaluated using the same diffusion equation with the sign of the left hand side reversed. After the partition functions are evaluated, the A-segment concentration is given by

$$\phi_A(\mathbf{r}) = \frac{V_c}{Q_c} \int_0^f \mathrm{d}s \; q(\mathbf{r}, s)\, q^\dagger(\mathbf{r}, s) \qquad (4)$$

where V_c is the diblock copolymer volume and $Q_c = \int \mathrm{d}\mathbf{r}\, q(\mathbf{r},s)\, q^\dagger(\mathbf{r},s)$ is the total partition function. Likewise, the B-segment concentration is obtained by evaluating the integral from f to 1.

We use infinitely long homopolymers to fill the air region surrounding the droplet. Their partition function, $q_h(\mathbf{r},s)$, satisfies the same diffusion equation (eqn (3)) subject to the homopolymer field, $w_h(\mathbf{r})$, but now s runs from 0 to ∞. In the limit $s \to \infty$, the ground state with the smallest eigenvalue λ becomes dominant[24,25] so that

$$q_h(\mathbf{r},s) \to \psi(\mathbf{r}) \exp(-\lambda s) \qquad (5)$$

Throughout this report, we calculate λ by evaluating $\partial q_h(\mathbf{r},s)/\partial s$ at $s = 4$, where the asymptotic expression, eqn (5), becomes accurate with a relative error of less than 1%. To calculate the homopolymer density, $\phi_h(\mathbf{r}) \propto \psi(\mathbf{r})^2$, we approximate the eigenfunction, $\psi(\mathbf{r})$, with $q_h(\mathbf{r},s)$ at the same s value.

For this work, it is essential to calculate the free energy of each morphology accurately, in order to identify the most preferable one. After self-consistency is satisfied, the free energy per block copolymer chain is

$$\frac{F}{k_B T} = -\ln\left(\frac{Q_c}{V_c}\right) + \lambda \frac{V - V_c}{V_c} + \frac{1}{V_c} \int \mathrm{d}\mathbf{r} \left(\frac{1}{2} \sum_{i \neq j} \chi_{ij} N \phi_i(\mathbf{r}) \phi_j(\mathbf{r}) - \sum_i w_i(\mathbf{r}) \phi_i(\mathbf{r}) \right) \qquad (6)$$

where V is the total volume of the system.

Even though we expect a locally periodic structure as a solution, the droplet–air surface inevitably breaks its long range periodicity. For the given situation, it is preferable to solve the diffusion equation in real space. It is natural to assume that the equilibrium morphology is symmetric with respect to the central axis of the droplet (see Fig. 1b). By adopting cylindrical

coordinates, ($r_\perp$, z, φ), the diffusion equation reduces to a 2-dimensional calculation which does not involve the φ coordinate. As we established earlier, the 2D diffusion equation is efficiently solved using the Crank–Nicolson finite-difference scheme with the alternate directions implicit (ADI) method.[20,26]

For the purpose of finding the self-consistent solution, iterations continue until the three field conditions, eqn (1) with i = A, B and h, and incompressibility, eqn (2), are satisfied. The pressure term, $\xi(\mathbf{r})$, in the field equation makes it a nontrivial task to create a new trial field from the previous output, and the convergence strongly depends on this choice. We slightly modify the method of Rasmussen *et al.*[27] which is a generalization of the Drolet–Fredrickson real-space method[28] for three segment species. Instead of adopting a field correction proportional to the individual $\delta\phi_i(\mathbf{r})$, we add $\zeta(\phi_{\text{tot}}(\mathbf{r}) - 1)$ to the output pressure field, where ζ is set to 3.0. Then output fields are created by inserting the output segment concentrations, $\phi_i(\mathbf{r})$, into eqn (1). The n'th input and output fields are mixed to create the $(n + 1)$'th input fields, $(1 - \varepsilon)w_i^{\text{in}} + \varepsilon w_i^{\text{out}}$, with a small dynamically-varying mixing ratio, ε. Anderson-mixing[20,29] is also applied at every 10th step to speed up the convergence, but we occasionally turn it off to ensure convergence. The iteration stops when the error measured by $\sum_i \int d\mathbf{r}(w_i^{\text{out}} - w_i^{\text{in}})^2 / \sum_i \int d\mathbf{r}(w_i^{\text{out}})^2$ is smaller than 10^{-18}.

We start solving the diffusion equation in a cylindrical region of radius $R = 16aN^{1/2}$ and height $Z = 16aN^{1/2}$. Then, as the droplet spreads, flatter cylinders up to $R = 40aN^{1/2}$ and $Z = 6aN^{1/2}$ are used. Regardless of the system size, we use a fine mesh with $\Delta r_\perp = \Delta z = 0.008aN^{1/2}$. For both block copolymers and homopolymers, 100 mesh points are used in the s direction. In the beginning of the iteration, block copolymers often stick on the top ($z = Z$) or side ($r_\perp = R$) surfaces, where no physical walls exist. To prevent this, our calculation starts by imposing repulsion on the top and side surfaces, but the repulsion is turned off after a physically sensible droplet appears.

The contrast between air–substrate and A-segment–substrate surface tensions is $\Delta\gamma \propto (\eta_A - \eta_h)$. We tune it by varying $\eta_A \geq 0$, while fixing $\eta_h = 0$. As we see later, if $\eta_B < \eta_A$, an A domain forms at the substrate, essentially prohibiting any B-segment–substrate contact. This justifies our choice of setting $\eta_B = 0$, leaving only one free parameter, η_A.

III. Results and discussion

Throughout this paper, we study a droplet of symmetric AB block copolymers, $f = 0.5$, with an internal interaction, $\chi_{AB}N = 20$. In bulk, they form a lamellar phase with period, $L = 1.694aN^{1/2}$. For a good comparison with the known experiment,[10] a large droplet with many internal lamellar periods is preferable, but numerical demands restrict its size. As a compromise, we consider a droplet of volume $V_c = 1152\pi a^3 N^{3/2}$, equal to a half sphere of radius $12aN^{1/2}$. This radius corresponds to approximately 7 lamellar periods. In the first two subsections, we present the droplet morphology for various parameter values. Afterwards, the identification of stable morphologies and the mechanism of morphological evolution are discussed.

A. Neutral air–surface interaction

We first consider the case with a *neutral* air–surface interaction, $\chi_{Ah}N = \chi_{Bh}N = 7.5$; *i.e.* the air is neutral with respect to the A and B domains. Fig. 2a shows the equilibrium droplet morphology for various η_A values. Each droplet consists of

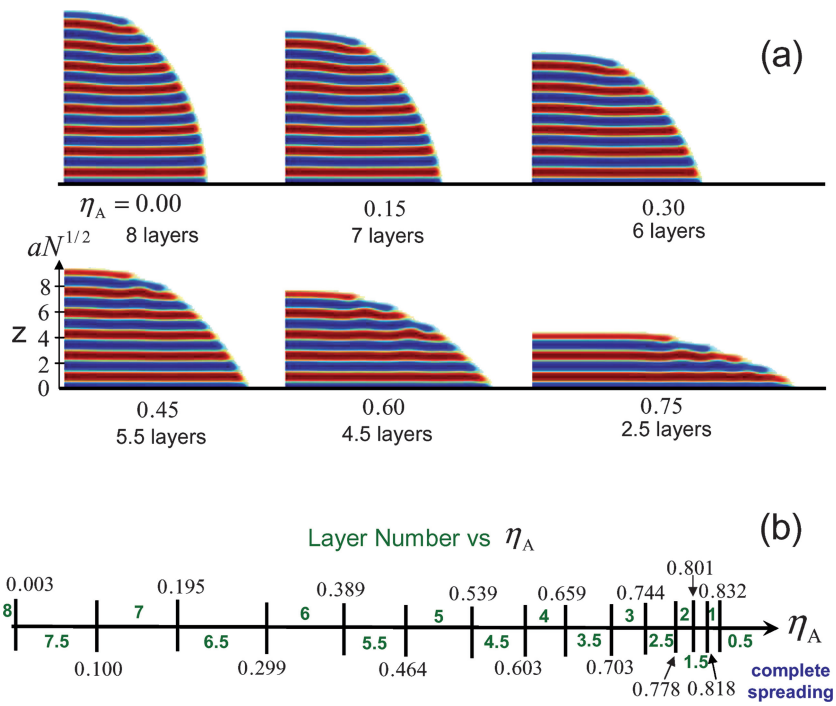

Fig. 2 (a) Vertical cross-section of AB diblock copolymer droplets with $\chi_{AB}N = 20$. The air is neutral to the block copolymer domains, $\chi_{Ah}N = \chi_{Bh}N = 7.5$. The droplet–substrate attraction parameter is $\eta_A = 0.00$, 0.15, 0.30, 0.45, 0.60, and 0.75. (b) A diagram showing the position of each layer number transition.

a stack of lamellar layers as observed in the experiment. As a natural consequence, the droplet height is *quantized* by the number of layers (periods). Because of the substrate selectivity, an A domain always occupies the bottom layer of a droplet. Thus, a droplet capped by an A (blue) layer exhibits integer number of layers, while half-integer number of layers are observed for a droplet capped by a B (red) layer.

The upper left droplet of Fig. 2a corresponds to the case of $\Delta\gamma = 0$. If it were a simple droplet without any internal structure, the contact angle (see eqn (7)) would be $\pi/2$, and an exact half sphere would be observed. The contact angle is indeed very close to $\pi/2$, but interestingly, the droplet exhibits eight layers, one layer more than what the simple estimation suggests; *i.e.* the vertical size of the droplet is larger than its horizontal size by about 20%. It implies that the block copolymers prefer to create less curved lamellar layers of similar lateral sizes, rather than creating spherically bent lamellar layers.

Apart from such deviations, the droplet shapes are approximately spherical at small η_A values. As η_A increases, the droplet spreads and the layer number decreases correspondingly. The 8-layered morphology changes to a 7.5-layered one at $\eta_A = 0.003$, then a transition to 7 periods happens at $\eta_A = 0.100$. Subsequent transitions are listed in Fig. 2b. It shows more frequent transitions at larger η_A, and the last few transitions occur almost simultaneously. After the last transition at $\eta_A = 0.832$, the spreading regime (0.5 periods) is observed, and the droplet does not spread further unlike the non-structured droplet which spreads until the disjoining pressure and other non-ideal effects stop it. This is due to the B block, which prefers to maintain its domain with the given spacing. As a result, the 0.5-layered morphology persists, at least for realistic parameter values.

A quantitative explanation of this critical η_A value for spreading is not available, but at least we can make a crude analytical estimation. It is straightforward to show that the surface tension contrast we impose by η_A is $\Delta\gamma = k_B T a \rho_0 \eta_A / \sqrt{N}$. If the A polymer length is infinite, the A-segment–homopolymer surface tension is known to be $\gamma_{Ah} = k_B T a \rho_0 \sqrt{\chi_{Ah}/6}$.[24,30] (Note the χ parameter, and hence the tension is the same for B segments.) The true surface tension must be lower than this due to the finite block copolymer length, but let us accept this value as an estimation of the droplet–air surface tension. The contact angle is then given by Young's equation,[31]

$$\cos\theta = \frac{\Delta\gamma}{\gamma_{Ah}} = \eta_A \sqrt{\frac{6}{\chi_{Ah} N}} \tag{7}$$

The contact angle vanishes at $\cos\theta = 1$, which gives 1.118 as the critical η_A value. It is about 35% larger than the actual value, 0.832; hence, this simple estimation only provides a qualitative prediction, and a full SCFT calculation is necessary for the quantitative understanding of the system. Moreover, the detailed features of the droplet, such as the wave-like kinks in the lamellar layers near the droplet–air surface, are only accessible by this full calculation.

The droplet shape deviates from the spherical one as η_A increases, but it is difficult to identify its exact geometry due to its small size. The side surface seems to be closer to a spherical curve, though it is not clearly distinctive from a hyperbolic shape which exhibits almost equally spaced steps. In summary, our calculation supports part of the experimental findings, but there are some significant differences.

B. Selective air–surface interaction

In experiments, it is practically impossible to find a diblock copolymer system completely neutral to air. Whichever diblock copolymer one uses, the air is likely to favour one block over the other so that the interaction becomes *selective*. We investigate the effect of selectivity by using block copolymers with different interaction parameters, $\chi_{Ah}N = 12.5$ and $\chi_{Bh}N = 7.5$. The droplet morphologies analogous to Fig. 2a are displayed in Fig. 3a. A major change from the neutral droplet case is that a droplet is always covered by a B (red) layer. The cap maintains a large contact area with air, and hence prefers the B layer which imposes lower interaction energy. This tendency combined with the fact that the bottom layer is always A, makes the layer number quantized to only half-integer numbers. Interestingly, the edge of each A layer maintains a small amount of area in contact with air even though it is enthalpically unfavorable. This observation indicates that the energy penalty of creating a highly curved surface layer and corresponding internal defects exceeds the possible surface energy gain, at least for our choice of parameters.

It is also noticeable that a selective droplet is flatter than the neutral droplet at the same η_A. At $\eta_A = 0$, the droplet has 6.5 periods which is 1.5 periods less than the neutral droplet, and its vertical size is smaller than the horizontal size by about 6%. Despite this, the overall droplet shape turns out to be less spherical than the neutral one. The droplets of Fig. 3a show a tendency to maintain large flat top layers, after which curved slopes follow to make contact with the substrate.

A simple qualitative argument explains this observation. The side surface of a droplet consists of the mixture of A and B domains. Its effective surface tension is therefore higher than that of the top surface which is covered by only a B domain. As a result, the droplet prefers to increase the top surface area while reducing the side surface area so that a faceted droplet is formed. Apart from the faceted surface, the droplet–air side surface shape is close to a spherical curve, though near the base of the droplet a hyperbolic fit might be possible.

The layer number transitions of selective droplets are listed in Fig. 3b. Overall, it is similar to the neutral case, except that only half-integer numbers of layers are accessible. Complete spreading happens at $\eta_A = 0.874$, slightly above the critical point of the neutral case. It is qualitatively explained from eqn (7) that the increase of the effective side surface tension will increase the critical tension. However, a quantitative analysis is even more challenging than for the neutral case.

C. Layer number transition

In the previous subsections, we considered only the equilibrium morphology. However, we have found many metastable morphologies, and it is essential to investigate these morphologies in order to fully understand the droplet behavior. As a typical example, we consider droplets of the neutral case,

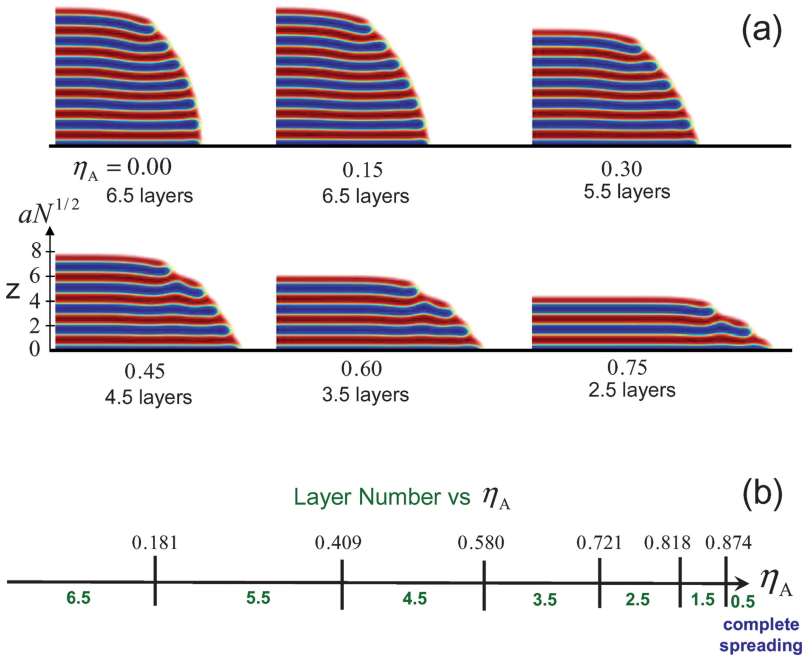

Fig. 3 Analogous plots to those in Fig. 2, but now with a selective air–surface interaction, $\chi_{Ah}N = 12.5$ and $\chi_{Bh}N = 7.5$.

around $\eta_A = 0.30$. The free energy curves displayed in Fig. 4a show that there exist two distinct 6.5-layered phases. The difference in the free energy per chain is very small, typically of order $10^{-4} k_B T$ or less, but our SCFT method with a fine mesh maintains a sufficient resolution to distinguish this difference.

The geometrical difference between the two phases is clearly visible. The two morphologies at $\eta_A = 0.27$, where their energies cross over, are shown in Figs. 4b and 4c. The droplet of $I_{6.5}$ has a larger top layer, while the 2nd layer from the top is larger for $II_{6.5}$. The bottom layer size of $I_{6.5}$ is only 0.5% smaller than that of $II_{6.5}$, but it is sufficient to make $I_{6.5}$ the preferable phase at small η_A (<0.27), while $II_{6.5}$ has a lower energy at larger η_A. $I_{6.5}$ eventually experiences a first-order phase transition to $II_{6.5}$ at $\eta_A = 0.33$, but before then, at $\eta_A = 0.299$, the energy of a 6-layered phase, I_6, becomes lower. Finally, above $\eta_A = 0.322$, another 6-layered phase, II_6, is favored. Even though the free energy comparison identifies the most preferable geometry, every other morphology is also a valid metastable solution. A droplet eventually loses its top layer as η_A increases, but it does not occur immediately after the morphology becomes metastable. This observation suggests that an experimental droplet may exhibit a metastable morphology, especially when the droplet is spreading.

Similar behaviors are observed for transitions to other layer numbers. Usually, two or more phases with the same layer number compete, and they often branch or merge without a definite pattern. In order to identify as many phases as possible, we increase and decrease the η_A value, and we very often use a neutral morphology as an input of the selective case and vice versa. Because 7.5- and 8-layered droplets do not appear from simple initial fields, we construct them by specifically manipulating $\chi_{Ah}N$ and $\chi_{Bh}N$. Nevertheless, these structures turn out to be stable near $\eta_A = 0$. We cannot guarantee that all the possible morphologies are explored. However, considering the small energy difference between phases with the same layer number, we are confident that the transition points in Figs. 2b and 3b are accurate to within ± 0.01.

The real-space SCFT method of Drolet and Fredrickson[28] originally suggested that one should start from a random field configuration to find an unbiased solution. Our calculation shows that the droplet obtained by this method always exhibits strongly curved lamellar layers, and defects are generated to fill in the droplet volume. Only when we start from periodic fields resembling those of the final solution, a droplet with well-aligned lamellar layers is created. Nevertheless, its free energy is significantly lower than those obtained from the random initial fields, and thus it is the equilibrium structure. Again, we cannot exclude the possibility that a real droplet is trapped into such a defect-filled geometry, especially when the morphology is frozen without much annealing.

IV. Comparison with experiments

In their experimental report, Croll *et al.*[10] showed that the side surface of the droplet fits well to a hyperbolic shape. However, the droplets in our numerical SCFT are faceted with spherical side surfaces. Indeed, some of the experimental droplets exhibit faceted shapes, but their side surfaces still fit better with hyperbolic curves.[32] In this section, we investigate this discrepancy by comparing the experimental and theoretical situations.

Let us first consider the parameter differences. PS-PMMA block copolymers are used in the experiment, and their surface tensions with respect to air are $\gamma_{PS-Air} = 31.2$ dyne/cm and $\gamma_{PMMA-Air} = 31.4$ dyne/cm at 150 °C,[33,34] which is the approximate annealing temperature. The difference is only 0.2 dyne/cm, but the experiment has observed that the PS layer

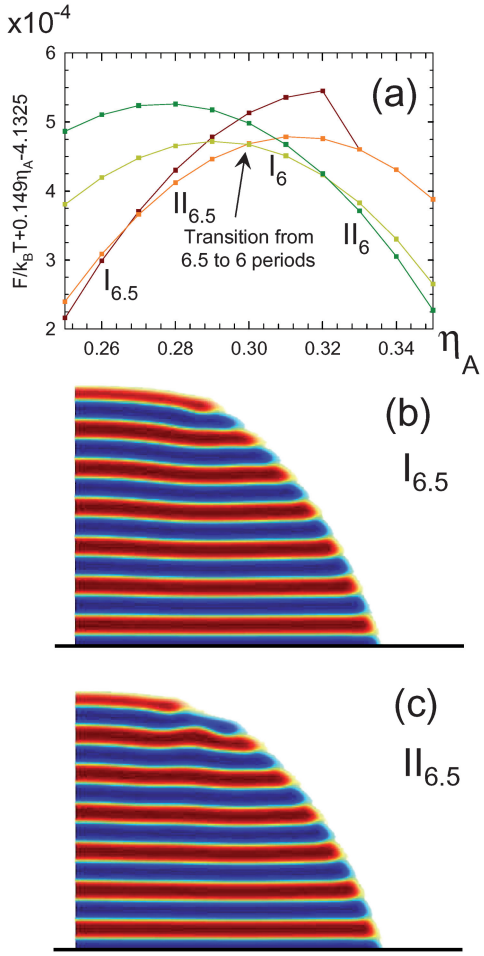

Fig. 4 (a) Free energy plot of four competing morphologies around $\eta_A = 0.3$. A linear term, $0.149\eta_A$, is added to clarify the transitions. Two 6.5-layered phases ($I_{6.5}$ and $II_{6.5}$) compete at lower η_A and two 6-layered phases (I_6 and II_6) are favoured at larger η_A. The transition from 6.5- to 6-layered phase occurs at $\eta_A = 0.299$. (b) and (c) display two 6.5-layered morphologies competing at $\eta_A = 0.27$.

always stays on top; hence the tension difference should not be ignored. The PS-PMMA surface tension in the limit of large molecular weight is $\gamma_{PS-PMMA} = 1.5$ dyne/cm,[34] and it decreases at a finite molecular weight; thus the inter-layer surface tension is at least one order of magnitude smaller than the droplet–air surface tension. Unfortunately, such an extreme tension ratio is troublesome in the SCFT calculation, because much finer grids are required at larger χN values. In order to test if the increase of the droplet–air surface tension makes the droplet more hyperbolic, we investigate a droplet with a small selectivity difference, $\chi_{Ah}N = 26$ and $\chi_{Bh}N = 25$. Figs. 5a and 5b display the droplet morphology at $\eta_A = 1.5$ and 1.7, respectively, and they show that the side surface of the droplet becomes more spherical as χN increases. It is a natural result considering that the strong surface tension highly penalizes a droplet with a non-spherical shape. We cannot see any reason for this trend to reverse at higher χN values.

The simple model of Croll *et al.* is based on an assumption that the lamellar layers are parallel to the substrate, and the side

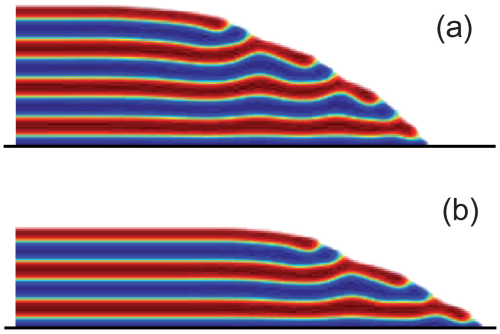

Fig. 5 Droplet geometries when the polymer–air surface interaction is slightly selective, $\chi_{Ah}N = 26$ and $\chi_{Bh}N = 25$, and they both exceed the internal surface interaction, $\chi_{AB}N = 20$. The droplet–substrate attraction is (a) $\eta_A = 1.5$ and (b) 1.7.

surface shape is terraced. Interestingly, Fig. 5 exhibits a smooth spherical surface rather than a terraced one, and the layers are not parallel to the substrate near the polymer–air surface. In terms of the surface energy, this geometry imposes less energy penalty than the terraced one, but the droplet instead develops tilts and kinks of layers which propagate into the droplet. They will impose a deformation energy penalty which is approximately proportional to the air-exposed layer area experiencing the deformation. The droplets in the experiment have aspect ratios greater than 10, and thus each layer has a large area subject to the deformation. We speculate that the increase of the deformation energy may eventually become dominant, and it will force the air-exposed layers to become parallel to the substrate forming flat terraces. The terraced geometry may in turn change the droplet shape to a hyperbolic one, as suggested by the simple model. In addition to the aspect ratio, the size difference between the experimental and theoretical droplets is also noticeable. The hyperbolic geometry becomes apparent only for large droplets, but numerical demands restrict our calculation to droplets with less than 10 layers. For such a small droplet, a somewhat curved droplet surface is often observed in the experiment,[32] though its exact geometry is difficult to identify because of its smallness and the faceted top surface.

There could be another explanation. The static contact angle between PS-PMMA block copolymer and the silicon substrate vanishes, and the droplet itself is dynamically spreading. The full spreading of the droplet typically takes a number of days, and hence the experimental report assumed that the droplet was effectively in equilibrium. However, it is also possible that the droplet dynamics prevent the true equilibrium structure. Even though our standard SCFT method does not include any dynamics simulation, it provides a few clues to this issue. A spreading droplet created by a sudden increase of η_A very often exhibits a near-hyperbolic side surface during the iteration of the field equations. Such a droplet is not in equilibrium, and the side surface shape finally converges to a spherical one, once the droplet spreads enough so that self-consistency is completely achieved. Although our iteration process does not represent the true dynamics, it still suggests that a hyperbolic droplet may survive when the droplet is spreading and in approximate equilibrium, but not in true equilibrium. Overall, we do not have

enough evidence regarding the role of droplet dynamics, and we must consider the possibility that a hyperbolic droplet may appear as an equilibrium structure for larger droplets with an extremely low contact angle.

It is interesting that our equilibrium droplet morphology resembles that of a smectic A liquid crystal droplet, suggesting that these two systems share the same physics of faceted droplet formation; *i.e.* the increase of surface energy due to exposure of layer edges could be the primary driving force determining the liquid crystal droplet shape. The experimentally observed liquid crystal droplet has hundreds of repeating layers and its contact angle is small with an aspect ratio of around 10.[12] Interestingly, its side surface is neither spherical nor hyperbolic. The faceted top surface is usually connected to a highly curved surface, but near the base of the droplet, the profile looks somewhat like a hyperbolic curve. Thus, it is possible that our curved droplet is only the upper part of a hyperbolic droplet observed in the experiment.

V. Conclusion

The present study shows the first quantitative calculation of the diblock copolymer droplet morphology on a free substrate. For the modeling, the air (or vacuum) region surrounding the droplet is replaced by infinitely long homopolymers, and the block copolymer–homopolymer system is solved using self-consistent field theory (SCFT) in a cylindrical coordinate system. For symmetric block copolymers ($f = 0.5$), a stack of nearly flat and circular lamellar layers appear inside the droplet; hence the layer number in the droplet is quantized. As the surface attraction between the droplet and the substrate increases, the droplet develops a nearly flat, faceted top surface, and its side profile is close to a spherical shape. This result is in contrast with the experiment of Croll *et al.*,[10] which reported a hyperbolic profile for a droplet with an extremely small contact angle. In such a droplet, where the aspect ratio is much larger than 10, the deformation of air-exposed layers imposes a significant internal energy penalty which may result in a hyperbolic geometry. This report also provides a clue to the structure and formation of smectic A liquid crystal droplets which assemble to create a faceted droplet with a curved side surface, much like our droplets. For the comparison with experiments, our calculations in this report are restricted to a narrow parameter region with symmetric ($f = 0.5$) diblock copolymers and a fixed volume, but this theoretical framework has the scope to model a wide range of polymeric systems without long range periodicity and explicit confinement.

Acknowledgements

We are grateful to Kari Dalnoki-Veress and Andrew Croll for discussion of the experimental result. This work was supported by EPSRC (Grants EP/D031494/1 and EP/F029616/1).

References

1 F. S. Bates and G. H. Fredrickson, *Phys. Today*, 1999, **52**, 32–38.
2 M. W. Matsen and M. Schick, *Phys. Rev. Lett.*, 1994, **72**, 2660–2663.
3 M. W. Matsen and F. S. Bates, *Macromolecules*, 1996, **29**, 7641–7644.
4 K. C. Daoulas, M. Müller, J. J. de Pablo, P. F. Nealey and G. D. Smith, *Soft Matter*, 2006, **2**, 573–583.
5 J. Y. Cheng, C. A. Ross, H. I. Smith and E. L. Thomas, *Adv. Mater.*, 2006, **18**, 2505–2521.
6 S. O. Kim, H. H. Solak, M. P. Stoykovich, N. J. Ferrier, J. J. de Pablo and P. F. Nealey, *Nature*, 2003, **424**, 411–414.
7 T. G. Fitzgerald, F. Borsetto, J. M. O'Callaghan, B. Kosmala, J. D. Holmes and M. A. Morris, *Soft Matter*, 2007, **3**, 916–921.
8 H. Xiang, K. Shin, T. Kim, S. I. Moon, T. J. McCarthy and T. P. Russell, *Macromolecules*, 2004, **37**, 5660–5664.
9 P. Chen, H. Liang and A. C. Shi, *Macromolecules*, 2008, **41**, 8938–8943.
10 A. B. Croll, M. V. Massa, M. W. Matsen and K. Dalnoki-Veress, *Phys. Rev. Lett.*, 2006, **97**, 204502.
11 J. Bechhoefer and P. Oswald, *Europhys. Lett.*, 1991, **15**, 521–526.
12 P. Oswald and L. Lejcek, *Eur. Phys. J. E*, 2006, **19**, 441–452.
13 D. N. Theodorou, *Macromolecules*, 1989, **22**, 4578–4589.
14 D. G. Peck and K. P. Johnston, *Macromolecules*, 1993, **26**, 1537–1545.
15 A. Hariharan and J. G. Harris, *J. Chem. Phys.*, 1994, **101**, 3353–3366.
16 L. Schlangen, F. A. M. Leermakers and L. K. Koopal, *J. Chem. Soc., Faraday Trans.*, 1996, **92**, 579–587.
17 F. Schmid, *J. Phys.: Condens. Matter*, 1998, **10**, 8105–8138.
18 K. C. Daoulas, D. N. Theodorou, V. A. Harmandaris, N. C. Karayiannis and V. G. Mavrantzas, *Macromolecules*, 2005, **38**, 7134–7149.
19 F. Schmid, *J. Chem. Phys.*, 1996, **104**, 9191–9201.
20 J. U. Kim and M. W. Matsen, *Macromolecules*, 2008, **41**, 246–252.
21 J. U. Kim and M. W. Matsen, *Phys. Rev. Lett.*, 2009, **102**, 078303.
22 M. W. Matsen, *Macromolecules*, 2006, **39**, 5512–5520.
23 S. F. Edwards, *Proc. Phys. Soc. London*, 1965, **85**, 613.
24 M. W. Matsen, in *Soft Matter, Vol. 1: Polymer Melts and Mixtures*, edited by G. Gompper and M. Schick, Wiley-VCH, Weinheim, 2006.
25 M. A. Moore, *J. Phys. A: Math. Gen.*, 1977, **10**, 305–314.
26 W. H. Press, S. A. Teukolsky and W. T. Vetterling, *Numerical Recipes in C: the Art of Scientific Computing*, Cambridge University Press, Cambridge, UK, 1993.
27 K. Ø. Rasmussen and G. Kalosakas, *J. Polym. Sci., Part B: Polym. Phys.*, 2002, **40**, 1777–1783.
28 F. Drolet and G. H. Fredrickson, *Phys. Rev. Lett.*, 1999, **83**, 4317–4320.
29 D. G. Anderson, *J. Assoc. Comput. Mach.*, 1965, **12**, 547.
30 E. Helfand and Y. Tagami, *J. Chem. Phys.*, 1972, **56**, 3592–3601.
31 T. Young, *Phil. Trans. R. Soc. London*, 1805, **95**, 65–87.
32 K. Dalnoki-Veress, personal communication.
33 J. Brandrup, E. H. Immergut and E. A. Grulke, *Polymer Handbook*, 4th edn, Wiley, New York, 1999.
34 S. Wu, *J. Phys. Chem.*, 1970, **74**, 632–638.